STRATIGRAPHIC PROFILING WITH GROUND-PENETRATING RADAR IN PERMAFROST: POSSIBLE ANALOGs FOR MARS

Steven A. Arcone
U. S. Army Cold Regions Research and Engineering Laboratory
Hanover, NH 03755

Abstract

In this review I discuss my experiences with using ground-penetrating radar to investigate permafrost in Alaska and in the Dry Valleys of Antarctica. The results may be relevant to radar efforts on Mars because of possible ice-rich conditions there. My surveys used pulses centered at 50-, 100- and 400-MHz. I interpret possible outwash and lacustrine deposits, and thermal imprints of migrated freeze fronts at two sites in Eastern Taylor Valley, Antarctica. Maximum depth of stratigraphy profiled was about 35 m in the Dry Valleys with about 30 m penetration in lacustrine sediments. Near Fairbanks, Alaska, I interpret depth of penetration at 50 MHz to be near 80 m in marginally frozen and stratifed alluvial sands. At other Fairbanks sites I found it difficult to differentiate between reflections from conductive bedrock, a graphitic schist, and those from the water table at depths of 20–35 meters. At a site on the North Slope of Alaska, I interpret thaw zones and remnant freezing fronts in an alluvial flood plain. The relative permittivity of the permafrost at most sites appears to range between about 4–5.5, which is consistent with felsic mineralogy mineralogy and low ice content. Weak interface reflectivity may have limited our interpretation of maximum penetration because high signal to noise ratios occurred at maximum reflection depths, signal absorption should have been low, and scarce diffractions imply that scattering was weak. The interface reflectivities beneath Taylor Valley may be a function of only density contrasts, since free water, and possibly ice, is absent. Obtaining similar results with a lower frequency air- or space-borne survey on Mars will be limited by the loss in resolution, possible increased signal absorption rates from Maxwell-Wagner-Debye type relaxations, and severe refraction of reflected signals as they cross the ground surface.

INTRODUCTION

The prospect of success in using ground-penetrating radar (GPR) for the detection of ice and water related features on Mars must rely heavily on Earth GPR exploration in permafrost terrain. Since 1992 I and colleagues at CRREL have conducted extensive GPR studies of permafrost in the Fairbanks, Alaska area, the North Slope of Alaska, and in the Antarctic Dry Valleys. These areas may serve as martian analogs because of the lack of unfrozen water due either to very cold temperatures (Dry Valleys), or to the coarseness of the sediments. Obviously, GPR interpretations are possible because of the existence of reflecting strata. In the examples I present here, I show stratigraphy that I have interpreted to characterize the presence of ice and former presence of water. I used a conventional commercial GPR system operating at 50–400 MHz. My examples also show the ability of GPR to penetrate permafrost; deeper penetration is inferred from signal-to-noise ratios.

I used a transient type pulsed GPR. Relative to modern ordnance radars, these systems do not provide high performance, mainly because of the low gain antennas and internal noise generated by the sample and hold technology used for converting RF energy to audio range for digitization (performance figure is about 120–150 dB). Current developments by commercial and academic institutions will improve system performance by using either low noise FM-CW or front-end digitizing pulsed systems and extensive trace stacking. We travelled to the antarctic sites by helicopter; the sites in Alaska were easily accessible by an all terrain vehicle. We fixed our position and elevation with 10-cm accuracy differential GPS in Antarctica. We correlated photographic, borehole and test pit information with the GPR results.

As with Mars, we expected that density or mineralogy differences in Antarctica might provide the only contrast in relative permittivity, ε, between depositional horizons because of the lack of unfrozen water content (mean, near-surface ground temperature is –18°C), and unknown ice content. In Alaska, it is more plausible that differences in ice content, in concert with differences in grain size, aided the stratification. Of equal concern in Antarctica were the 20–50 cm surface rocks, which made traversing difficult. Similar distributions at depth could cause scattering loss and clutter.

To my knowledge GPR results for the Dry Valleys have only been reported by us (Arcone and Delaney, 2000) for work done in 1998. The sediments we have profiled are stratified silts, sands and gravels of low or little ice content, virtually no water, and either of glacio-fluvial or glacio-lacustrine origin. The stratigraphy and 30 m of penetration previously achieved in deltaic, well drained sands and gravels in a presently arid environment using 50- and 100-MHz GPR (e.g., Johl and Smith, 1991) encouraged our work; profiles of sand deposits in more temperate or tropical environments generally show less than 20 m of penetration (Bristow et al., 2000). We have also yet to find any reported GPR profiles of lacustrine layering of silts and clays, but this may reflect the high rates of attenuation associated with these sediments when wet. The penetration I interpret in lacustrine silts strongly suggest a very dry state.

EQUIPMENT AND METHODS

We used the portable, battery-powered GSSI 16-bit System 2 control unit and 400-MHz (model 5103 at 1.7 W peak power) and 100-MHz (model 3207 at 800 W peak power) antennas (**Fig. 1**) polarized transverse to the transect directions. We constructed our own 50-MHz resistively loaded dipoles with which we used the GSSI 100-MHz transmitter and receiver. We hand-dragged the antennas along the rough, Dry Valleys terrain, and used a vehicle over snow laden trails in Alaska (**Fig. 1**) while recording continuously at data acquisition rates of 24 to 48 traces per second. The 1- and 2-m width of the 100- and 50-MHz antennas forced us to set many rocks aside and choose our paths carefully in Antarctica to avoid antenna-ground decoupling noise. We generally recorded with range gain at 120 ns (400 MHz), 500–700 nanoseconds (ns) at 100 MHz and 1000–1500 ns at 50 MHz.

Our post-processing was performed with WINRAD (GSSI) software. We used high and low pass noise filtering, automatic gain control, and, for some records, deconvolution. The automatic gain control equalizes gain across the time traces of a record, which can bring out weak reflections, but at the expense of amplifying noise. The deconvolution used a predictive lag of one cycle, effectively reduced the transmitted pulse by about ½ cycle, and altered the phase sequence of half-cycles in the waveform. After applying positional and elevational corrections, we migrated some records using a two-dimensional Kirchhoff time-migration scheme. Diffractions in these records, assuming point sources, give dielectric constants of about

4–5.5. These are realistic values for primarily felsic frozen sands and gravels. The limited penetration of 35–80 m, and the nearly flat lying stratigraphy make me reasonably sure that a more correct, three dimensional migration approach would not significantly improve the results.

Our radar control systems are of commercial grade and utilize sample-and-hold technology to convert RF energy to audio range for digitizing. Recent circuitry improvements for this procedure may have eliminated much of an estimated 40 dB that used to exist in the system noise floor. Since conventional GPR is transient in nature, there is an additional noise problem caused by the wide bandwidth receiver. Glacial profiles I have recently obtained in Antarctica with this system (Arcone et al, 2001) suggest that signals with about 136 dB of loss may be detectable with high rates of stacking in more advanced commercial systems. The antennas are usually mounted in a parallel and opposing configuration (**Fig. 1**), which places the maximum antenna gain in the profile direction (Arcone, 1995). This orientation is often inconvenient for conventional towing because the antennas catch on rocks, lift off the surface and cause resonance throughout the record.

DRY VALLEYS PROFILES

The Dry Valleys of Antarctica cover about 4000 km^2. The polar desert climate and mountain blockage of outflow of the East Antarctic ice sheet now keeps the valleys snow and ice free throughout the summer months. Ice-bonded, or dry permafrost may be up to 600 m deep, and the area is often compared with possible conditions on Mars. As with Mars, the origin of many features of the valley geomorphology is controversial. Two vastly different points of view exist concerning the long-term evolution of the valleys. Stabilists argue that the valleys formed largely through fluvial erosion (Denton et al., 1993; Sugden et al., 1995) prior to 20 million years ago, and were preserved since at least 14 Ma in a polar-desert climate or beneath continuous, frozen-bottom ice advances. This implies minor glacial erosion because of the lack of bottom sliding. Dynamicists argue for significantly fluctuating climate and ice-sheet glaciation over much of the last 40 million years. They would argue for wet-based ice advancements into the Dry Valleys, characterized by episodes of melting (Webb et al., 1996; Prentice and Matthews, 1991), such as during the Pliocene (2–5 ma). This scenario implies glacial sliding and repeated episodes of major glacial erosion and fluvial deposition. If this latter case is true, then diagnostic stratigraphy of fluvial origin should be commonly uncovered with GPR and would make this possible martian analogy all the more relevant.

Our antarctic sites are located in eastern Taylor Valley (**Fig. 2**). The sites include Hjorth Hill, which is at the ocean-end of Taylor Valley on the northern valley wall, and the Sloth Lake area, which is farther west, near Lake Fryxell. These sites contain hummocky features that appear to be part of a morainal surface. They revealed the most stratigraphy during our two seasons of study. Erosion may have removed much of the stratigraphy at other sites we investigated (Arcone et al., 2000). The uneven nature of the terrain made dragging the antennas somewhat problematic, and several of our profiles were completed in sections. Weather during all our investigations was always clear, breezy, and with temperatures between about –5 and 0^0 C.

The elevated strand lines throughout the valley and the widespread occurrence of silty deposits along the lower valley walls leave little doubt that a lake (Glacial Lake Washburn) up to several hundred meters deep existed there during the Holocene (Green and Friedman, 1993). Although hundreds of 1-m deep pits have been obtained throughout the Dry Valleys, to date, only about 12 deep holes (80–300 m within Taylor Valley; McKelvey, 1981) have been drilled and there is no prospect for near future drilling because of environmental concerns.

Sloth Lake

This area contains numerous elongated mounds (**Figs. 3,4**) of a few meters in height, up to about 80 m in cross sectional length, and oriented primarily transverse to the valley axis in a NE–SW direction. The ridge morphology and the surface veneer of volcanic debris derived from across McMurdo Sound suggest that they might be minor recessional moraines deposited at the grounding line of a lobe of the West Antarctic Ice Sheet from the East. Several other origins have been considered (Denton et al., 1989; 1991).

Figures 5 and 6 show profiles that crossed two of these mounds in the north-south directions. The 100-MHz profile in **Figure 5** shows mainly horizontal reflection horizons, parts of which are discernible in the lower part of the profile to about 38 m depth between 0 and 95 m distance. I interpret these horizons to

represent bedding of Glacial Lake Washburn. Near the top, especially from 0–80 and 150–190 m, is faint evidence of dipping beds, which are well profiled at 400-MHz (**Fig. 6**).

The 400-MHz profile of **Figure 6** along with many others, was recorded at a time range of 120 ns. It shows a series of sigmoidally shaped foreset beds to a depth of about 6 m. They are crossed by scalloped shaped erosional surfaces, the most prominent of which occur between 0 and 80 m. Beneath these beds are the more continuous lacustrine horizons, which also appear between 200 and 245 meters. The few diffractions in this and other records indicate relative dielectric permittivities of 5.5, which is consistent with ice-bonded sands and gravels (Arcone et al, 1998a; Arcone et al., 1998b). Many of these reflections are characterized by simple wavelets, which indicate isolated interfaces. In some cases there are faint, extended cycles which indicate the bottom reflection of a thin layer. Each wavelet has a characteristic phase, which we define as the polarity (plus or minus) sequence of the amplitude dominant central three half-cycles (Arcone et al., 1995). Red bands indicate positive phase polarity and blue indicates negative. The profile has not been deconvolved, so that the phases of the reflected wavelets are retained through the porcessing. For this particular model antenna, a red-blue-red sequence indicates a reflection from an interface between a material of higher dielectric permittivity (and density) over one of lower, and vice versa. Higher permittivity would be caused by interstitial filling of sand grains by silt or ice, so that higher permittivity corresponds with higher bulk density, and vice versa.

The steepness of the foreset slopes is an artifact of the horizontal compression I used for display. In fact, the slopes are on the order of $10\text{-}20^0$, and far less than the asymptotic slope of a hyperbolic diffraction (shown in the figure). For this reason, the processing procedure of wave migration (used for converting the distance vs. time record into a proper distance vs depth record) does not improve the image, as seen in the figure.

The scalloped shaped horizons are of particular interest because they appear to be secondary thermal features superimposed on the bedding. Edgewise viewing shows that the phase bands and slope of the bedding reflections are continuous across them. The scalloped horizons are characterized by a blue-red-blue phase sequence, which indicates an interface between lower density material (e.g., ice) above, over higher density material (e.g., icy sand and gravel) below. They are also characterized by faint, trailing, extra cycles that indicate thin layers. Therefore, these features may represent ice layers that formed at stalled freezing fronts that had migrated downwards through the foreset beds. The scallop shape may have resulted from the beds having had higher heat conductivity than surrounding silts that have since been eroded away, and so the frost boundary migrated deeper within them.

Presently, I and my colleague Mike Prentice at the University of New Hampshire believe that these foreset deposits are outwash from meltdown of the West Antarctic Ice Sheet that traveled from West Antarctica across the Ross Sea and terminated at the mouths of the Dry Valleys. Some of the evidence for this are the volcanic erratics dispersed about the heads of the Dry Valleys and which appear to have been picked up from Ross Island.

Hjorth Hill

This site (**Fig. 7**) is located at the eastern end of Taylor Valley (**Fig. 2**) on a prominent lateral moraine overlooking the Ross Sea. The top of the hill is bare metaigneous rock. It is currently debated as to whether the lateral moraine is single or multiple and whether it was deposited in conjunction with the West Antarctic Ice Sheet or with expansion of local piedmont glaciers. The mound of sediment we profiled was about 500 meters across and contains a small basin.

Figure 8 shows 100-MHz profiles of parallel transects that went from south to north (left to right in the photo of **Fig. 7**) and crossed both edges of the moraine complex. Uphill is to the left. Each profile contains two prominent horizons, the lower of which dips down hill to a depth of about 30 meters beneath the mound peak in the upper profile. The upper horizon is more horizontal and has a maximum depth of about 15 m beneath the peak. Between these two horizons occur faint horizontal horizons that are more visible when the profile is viewed edgewise. The strongest events appear beneath the mound peak, and the signal to noise ratio of one of them is at least 4 (the “noise” is taken to be the peak value of events close by in time). In contrast, the 50- and 100-MHz profiles along one east-west transect over the same mound at 350–400 m and compared in **Figure 9** show only a slight dip in the deepest horizon (especially when considering the vertical exaggeration), and in several nearly horizontal horizons above it.

The south–north dipping horizons of **Figures 8 and 9** may be an erosional surface, and the horizontal horizons may be lacustrine sediments that were deposited as outwash in a lake dammed by the Ross Sea ice

advance, which is known to have reached up this hill. This lower horizon may represent bedrock. Although the 50-MHz profile of **Figure 9** gives a stronger response to most of the horizons, it is apparent that the deepest events seen at 50 MHz are also seen at 100 MHz. Therefore, any losses caused by scattering could not be significant at these frequencies because scattering losses are proportional to the fourth power of the frequency. Given that losses caused by water or mineralogic relaxations are not significant, this leads us to conclude there are probably no further interfaces.

INTERIOR ALASKA PROFILES

Alluvial floodplain deposits are extensive between the present Tanana River and the foothills of the Alaska Range; Fort Wainwright alone covers 665,000 acres and is only a small part of this area. These areas contain much sand and gravel for which attenuation rates at 100 MHz are about 0.5–1.0 dB/m (Arcone and Delaney, 1989). In contrast, the uplands area around Fairbanks are covered with loess and reworked silt deposits up to 100 m thick in the valleys, and are usually ice-rich. All these areas contain discontinuous permafrost. CRREL has conducted numerous radar studies in the silty deposits, including extensive profiles along all the major roads of the Fairbanks area.

The Fairbanks sites I discuss are located on Fort Wainwright, just north of the Chena River (**Fig. 10**). The sites are within the floodplain of the Chena River and Tanana River complex. GPR investigations throughout this area are discussed by Arcone et al. (1998b). Typical summer and winter permafrost conditions are diagrammed in **Figure 11**. The permafrost here is in marginally frozen alluvial deposits; temperatures are within one degree celsius of zero. The active layer (surface layer of seasonal freezing) is at least 1.5 m thick and usually composed of saturated silts, organics and fine sands. Bedrock, a highly conductive, quartz-mica graphitic schist, is generally about 30–260 m deep throughout the area.

The area in general transports subpermafrost water by aquifers because in many places permafrost is frozen into bedrock. However, the bedrock itself is highly reflective and makes for difficult interpretation of aquifers because it is a graphitic schist with a dielectric constant of about 11 and a conductivity that may be greater than 0.01 S/m. Consequently we haved used GPR as a method to find candidate aquifers, which we later verify by drilling.

In general, there is almost no apparent penetration in the silty and ice-rich permafrost of the uplands at any frequency that we have tried (50–400 MHz). These results have helped to feed the present paradigm that silts and clays, frozen or not, afford little penetration to GPR signals. However, I am presently researching attenuation rates in silts and find that one-way values at about 400 MHz are around 7 dB/m for a volumetric water content of about 6%, which is typical for the loosely packed near-surface loess deposits that drape the hillsides. Although this is high loss rate, it does not preclude penetration of several meters. The lack of apparent penetration may be more a result of a lack of continuous interfaces in the reworked silt.

Subpermafrost groundwater

Figure 12 shows two perpendicular 50-MHz profiles recorded at site 1, located in **Figure 10**. The interpretation in the figure is for profile 6 and is aided by eight well logs. This profile appears to cross several aquifers, one of which we were lucky enough to profile along transect 96. Profile 6 is filled with reflections and diffractions; without drilling we could not distinguish bedrock reflections from groundwater reflections. Despite the uniform value of 5.4 that we determined for the bulk permafrost dielectric constant, the diffractions indicate a large degree of inhomogeneity. Their presence however, also indicates that single scattering occurred.

Deep permafrost

I show a 50-MHz (system shown in **Fig. 1**) profile in **Figure 13** that shows the deepest returns of which I am aware for any land-based GPR profile**.** I recorded this profile at site 1 in **Figure 10** because the proximity of the Chena River suggested that permafrost might be shallow and underlain by the water table, as diagrammed in **Figure 11**. I applied automatic gain control (AGC) and additional low pass filtering to alleviate the noise that accompanied the AGC process. A water table provides strong reflections, but none are apparent in the profile. Instead, the profile shows stratification, no diffractions and deep returns. Subsequent drilling in 1995 found bedrock below 70 meters of ice-rich sand at the 90 m distance, no water table or the bottom of permafrost, but did encounter bedrock. Therefore, my depth calibration is based on

an estimated dielectric constant = 4 for ice-rich, felsic sands. The faint events indicated by arrows would then occur at about 80 m depth, and may indicate features near or beneath the bedrock surface.

NORTH SLOPE, ALASKA PROFILES

The Alaskan North Slope area is the piedmont and outwash zones located between the Brooks Range and the Beaufort Sea. The geology is generally stratified sands and gravels, but with marine deposits near the coast. Permafrost is about 600 m deep here and the active layer is about 30 cm thick. Nearer the coast about 40-50% of the land surface is covered by lakes of a few meters depth, and the ground itself is ice-rich. The lakes freeze to about 1.6 m depth (Arcone et al, 1997). There are many rivers that reach from the mountains to the sea, and their flood plains may be up to 6-10 km wide in places. The braided streams of these flood plains cut through the seasonally frozen flood plains, which become permafrost at a few meters depth. The Saganavirktok River runs through Prudhoe Bay.

From 1988 through 1993 CRREL conducted extensive GPR investigations of the flood plain areas of eight major rivers to help the Alaska Fish and Wildlife Service determine the water reserves that might be needed for oil drilling. The stratigraphy we found led to a GPR study of seasonal migration of freeze fronts associated with thaw zones beneath the rivers (Arcone et al, 1998a). The study area is between the Dalton Highway and Franklin Bluffs at about 25 km from Prudhoe Bay (**Fig. 14**). Gravel bars and icings give minor relief to the flood plain. Snow thickness generally ranged between 5 and 25 cm. The profiles were generally across the stream directions. One cannot identify any particular stream from the outdated topographic quadrangle maps.

The following examples are taken from Arcone et al (1998a) and were obtained in January and April, 1993. They focus on profiling the seasonal thaw "bulbs" that may exist beneath North Slope rivers. If such bulbs persist for more than one year they are known as taliks, which generally refer to persistent thaw zones within permafrost, whether above or below 0^0 C. If they are below 0^0 C they may be referred to as "cryopegs."

Control Lines

The profiles in **Figure 15** were obtained, along with drilling, to verify the presence of free water and to obtain talik depths in order to determine ε for the cyclically frozen ground above them. The reflections from the bottom of the channel ice and from the top surface of the talik have the same phase (tone sequence in their reflection bands) and are, therefore, from interfaces between materials of lower ε above, and of higher ε below. Intermittent reflections from the bottom of the talik are evident only in profile B. The hyperbolically shaped diffractions from within the taliks indicate an inhomogeneous permittivity structure. Weak reflections and diffractions throughout the frozen material indicate slight variations in its permittivity.

The drilling depths and reflection times give an ε between 4.5 and 5.5 near the ends of the taliks or where they are deeper. These values are typical for alluvial permafrost (Arcone and Delaney, 1989; Arcone *et al*., 1992) and represent an ice content of probably less than 20%. The lower values above the main part of the taliks in profile B indicate an ice content in excess of 70% (Delaney and Arcone, 1984; Arcone and Delaney, 1989). We interpret a decrease in drilling resistance encountered just before free water was reached at 33 m distance in profile A to indicate an ice layer, whose reflection is marked in the profile (event c). The free water from the talik rose approximately 60 cm above the ground surface and then settled to a slow trickle that lasted over 30 minutes.

Partial Freezing of a Talik

I compare cross-sectional profiles of a talik recorded in January and April 1992 in **Figure 16**. In January the talik was thickest beneath the deepest part of the channel, where it had just lost contact with the ice bottom. Only a small talik remained in April and a lower surface is barely discernible. The difference in phase between the talik top and bottom reflections (trace 385 in Figure 17) verifies the expected contrasts in ε across the interfaces. I interpret the reflection between distance points A and C within the January talik to be from the bottom of a partially frozen zone that extends to the talik surface. The relative strength of this reflection is seen in trace 311 of **Figure 17**. Partial freezing is also consistent with the

generally weaker strength of the talik surface reflection near point B where only 1.5 cycles are visible in the profile. The greater signal strength outside of points A and C, which makes all 2.5 cycles visible, is consistent with a completely unfrozen state. As seen in the previous example, there is evidence of an accretionary ice layer (event c in the profile) on the surface of the talik.

I show my values of ε and interpret the talik structures in **Figure 18**. I interpolated the control line calculations for the frozen sediments surrounding the upper surface of the talik in January to give ε values which linearly decreased from 4.7 at less than 2-m and greater than 40-m distances, to 3.7 near the center at 22 m. The 3.7 value corresponds with a volumetric ice content of about 73% (Delaney and Arcone, 1984). If this percentage held throughout the talik, I find that only about 1% of the remaining volume within the upper portion of the talik between points A and C needs to have been unfrozen water to have provided an ε = 4.7 (using the refractive index mixing model [Annan *et al*., 1994]) and to have generated the observed weak reflections with the proper phase. Most of the talik that I interpret to have been totally melted in January appears to have been less than 1 m thick and with a bottom surface of fairly uniform depth. The bottom surface appears to have moved about 1.3 m deeper by April. It is also possible that the April talik was partially frozen.

DISCUSSION

The deepest penetration in the Dry Valleys of about 40 m represents only the deepest interface that occurred. The signal to noise ratio of 4 in **Figure 9** implies that another 100 m could be penetrated and still provide a signal 3 dB above noise if only geometric attenuation of intensity further occurred. The lack of water in the sediments precludes the usual dc conductivity and Debye relaxation mechanisms as causes of signal attenuation. As opposed to the probable Martian situation, we doubt that magnetic (Olhoeft and Capron, 1994) and Maxwell-Wagner (Matzler, 1998) relaxation losses were significant because hematite, magnetite and any other conductive or magnetic minerals are a very small fraction of the soil (Claridge, 1965; Bockheim, 1997). The lack of diffractions within the 100-MHz profiles suggests weak ε contrasts between sediments and rocks, and a sparse volumetric distribution of larger rocks at depth. This is consistent with single scattering theory (Smith and Evans, 1972), which predicts only 8 dB loss over a round trip distance of 30 m for an estimated 10% volumetric content of boulders (as on the surface) with an ε = 8 (Ferrar dolerite; mainly calcium-rich feldspars at ε =7 and augite at ε = 7–10) and < 1/6 *in situ* wavelength in radius (< 25 cm) within the sedimentary matrix (minimum ε = 4). Therefore, weak contrasts in ε, and interface roughness may have limited the depth of our deepest detectable interface; actual penetration may have been far greater.

The scalloped shaped reflections at Sloth Lake may be uniquely related to the presence or former presence of ice because they seem to have been imprinted over the foreset stratigraphy, such as would result from a downward migrating freeze front. The presence of greater ice and therefore, ice bonding, may also be consistent with their association with topographic high points because such ice bonding would make these areas more resistant to erosion. If they are remnant freeze fronts then their presence implies the occurrence of warmer ground into which the fronts migrated. Warmer temperatures are also required to have allowed strong stream action to deposit these ridges of sand and gravel.

The penetration of 70–80 m in the Fairbanks area was possible because of the lack of silts or clays, which precludes the presence of any significant unfrozen water. In this case of frozen sands the temperature may be of little consequence to penetration so long as the ground is below freezing. In addition, the lack of gravel or cobbles should preclude any losses caused by scattering.

The situations shown in **Figures 12,15 and 16** are complicated, required drilling for complete interpretation, and represent cases where unfrozen water was present, probably even within the body of the Fairbanks permafrost and associated with silt. The contrast in dielectric properties between frozen and unfrozen water undoubtedly causes the stronger diffractions and reflections, and may even be the cause of the strong event seen at depth at Hjorth Hill (**Fig. 8**). In all these cases, such bright and complicated returns are local phenomena that could only have been detected with a detailed ground survey.

CONCLUSIONS AND RECOMMENDATIONS

Our conventional, transient type GPR system was able to penetrate at least 30 m in deeply frozen and probably dry silts, and about 80 m in ice-rich sands. Potential radar penetration in dry, felsic sediments could be greater than 100 m with more advanced type systems, such as those being developed by the University of Kansas. System performance is vastly improved by high rates of signal stacking. It is my experience that this process should be performed on the dynamic record; i.e., stacking is performed on traces recorded at consecutive spatial positions and not just at one position, to suppress clutter, as well as random noise. I think that colinear (e.g., Barbin et al., 1996) antennas for Mars surveying would avoid antenna decoupling, such as might occur when part of an antenna comes to rest on a rock.

Of all the examples I have presented, I find those of Figures 8 and 16 of possibly greatest relevance to the search for water on Mars. These profiles, the second for sure, illustrate unfrozen water responses from within very cold environments. They are far too localized for an airborne or spaceborne based radar to recognize. However, if such features are frequent, say in a suspect floodplain, then they could produce interesting speckle patterns in a ground surface image.

ACKNOWLEDGMENTS

This work was supported by NASA grant PIDDP 98-OSS-03, NSF grant OPP9725745, and the US Army DoD Work unit AT24-EP-004.

REFERENCES

Annan, A. P., Cosgrove, S. W., and Sigurdsson, T., 1994. GPR for snow pack water content. *Proc., Fifth Int. Conf. on Ground Penetrating Radar*, Kitchener, Ont., Ca., June 12–16.

Arcone, S.A., 1995. Numerical studies of the radiation patterns of resistively loaded dipoles. *Journal of Applied Geophysics*, **33**, 39–52.

Arcone, S.A., Chacho, E.F., Jr. and Delaney, A.J., 1992. Short-pulse radar detection of groundwater in the Sagavanirktok flood plain in early spring. *Water Resources Research*, **28**, 2925–2936.

Arcone, S.A. and Delaney, A.J., 1989. Investigations of dielectric properties of some frozen materials using cross-borehole radiowave pulse transmission. *CRREL Report 89-4*, U.S. Army Cold Regions Research and Engineering Laboratory, Hanover, NH, 18 pp.

Arcone, S. A., Chacho, E. F. Jr., and Delaney, A. J., 1998a. Seasonal structure of taliks beneath arctic streams determined with ground-penetrating radar, *Proc. VII Int. Conf. On Permafrost*, Yellowknife, N.W.T., Canada, June, 1998.

Arcone, S. A., Delaney, A. J., 2000. Stratigraphic profiling in the antarctic dry valleys, *Proc., Eighth Intl. Conf. on Ground-Penetrating Radar*, May 26–29, Gold Coast, Australia.

Arcone, S. A., Lawson. D. E., and Delaney, A. J., 1995. Short-pulse radar wavelet recovery and resolution of dielectric contrasts within englacial and basal ice of Matanuska Glacier, Alaska, USA, *Journal of Glaciology*, Vol. 41, No. 137, pp. 68–86.

Arcone, S.A., Lawson, D.E., and Delaney, A.J., Strasser, J. C., and Strasser, J. D., 1998b. Ground-penetrating radar reflection profiling of groundwater and bedrock in an area of discontinuous permafrost, *Geophysics*, Vol. 63, (5), 1573–1584.

Arcone, S. A., Lawson, D. E., Delaney, A. J., and Moran, M., 2000. 12–100 MHz depth and stratigraphic profiles of temperate glaciers, *Proc., Eighth Intl. Conf. on Ground-Penetrating Radar*, May 26–29, Gold Coast, Australia.

Arcone, S.A., Mayewski, P., and Hamilton, G., 2001. Stratigraphic profiling of the West Antarctica firn regime with 400-MHz GPR. Expanded abstracts, *Proc. 71st Annual Meeting, Society of Exploration Geophysicists*, San Antonio, Texas, Sept., 2001.

Barbin, Y. and 6 others., 1996. Radar for Mars soil sounding and testing results. In: *GPR '96, Proceedings of the Sixth International Conference on Ground-Penetrating Radar*, Sendai, Japan, Sept 30–Oct 3, 1996.

Bockheim, J.G., 1997. Properties and classification of cold desert soils from Antarctica, *Soil Science Society of America Journal*, Vol. 61, pp. 224–231.

Bristow, C. S., Best, J. L., and Ashworth, P. J., 2000. Use of GPR in developing a facies model for a large sandy braided river, Brahmaputra River, Bangladesh. *Proc., Eighth Intl. Conf. on Ground-Penetrating Radar*, May 26–29, Gold Coast, Australia.

Claridge, G.G.C., 1965. The clay mineralogy and chemistry of some soils from the Ross Dependency, Antarctica, *New Zealand Journal of Geology and Geophysics*, Vol. 8, pp. 186–220.

Delaney, A.J. and Arcone, S.A., 1984. Dielectric measurements of frozen silt using time domain reflectometry. *Cold Regions Science and Technology*, **9**, 39–46.

Denton, G.H., Sugden, D.E., Marchant, D.R., Hall, B.L., and Wilch, T.I., 1993. East Antarctic ice sheet sensitivity to Pliocene climatic change from a dry valleys perspective, *Geografiska Annalen*, Vol. 75A, pp. 39–41.

Denton, G. H., Bockheim, J. G., Wilson, S. C., and Stuiver, M., 1989. Late Wisconsin and early Holocene glacial history, inner Ross Embayment, Antarctica, Quaternary Research, Vol. 31, pp. 151–182.

Denton, G. H., Prentice, M. L., and Burkle, L. H., 1991. Cenozoic history of the Antarctic ice sheet, *in* Tingey, R. J., ed., *The Geology of Antarctica*, Oxford Monographs on Geology and Geophysics 17: Oxford, Clarendon press, p. 365–433.

Green, W. J., and Friedmann, E. I., eds., 1993. *Physical and biogeochemical processes in antarctic lakes*. Antarctic Research Series, Vol 59, American Geophysical Union, Wash. D. C.

Johl, H.M., and Smith, D.G., 1991. Ground penetrating radar of northern lacustrine deltas, *Canadian Journal of Earth Sciences*, Vol. 28, pp. 1939–1947.

Matzler, C., 1998. Microwave permittivity of dry sand, *IEEE Transactions on Geoscience and Remote Sensing*, Vol. 36, No. 1, pp. 317–319.

McKelvey, B.C., 1981. The lithologic logs of DVDP cores 10 and 11, eastern Taylor Valley, *Dry Valley Drilling Project, 33, Antarctic Research Series*, L.D. McGinnis, Ed., American Geophysical Union, Wash. D.C.

Olhoeft, G.R., and Capron, D.E., 1994. Petrophysical causes of electromagnetic dispersion. In: *GPR '94, Proceedings of the Fifth International Conference on Ground-Penetrating Radar*, Kitchener, Ontario, June 12–16, 1994.

Prentice, M.L., and Matthews, R.K., 1991. Tertiary ice sheet dynamics: the snow gun hypothesis, *Journal of Geophysical Research*, Vol. 96, pp. 6811–6827.

Smith, B. M. E. and S. Evans., 1972. Radio echo-sounding: Absorption and scattering by water inclusions and ice lenses, *Journal of Glaciology*, Vol. 11, No. 6, pp. 133–146.

Sugden, D.E., Denton, G.H., and Marchant, D.R., 1995. Landscape evolution of the Dry Valleys, Transantarctic Mountains: tectonics implications, *Journal of Geophysical Research*, Vol. 100, pp. 9949–9967.

Webb, P.,-N., Harwood, D.M., Mabin, M.G.C., and McKelvey, B.C., 1996. A marine and terrestrial Sirius Group succession, middle Beardmore Glacier Alexandria Range, Transantarctic Mountains, Antarctica, *Marine Micropaleontology*, Vol. 27, pp. 273–298.

APPENDIX

A REFRACTION CONSIDERATION FOR AIR OR SPACE BORNE RADIO SURVEYING

Air or spaceborne radio echo surveying needs to consider the effects of refractive focussing and defocussing caused by the contrast between the refractive indices of ground and space. Refractive focussing is commonly considered in airborne radioglaciology. Rays at the wider angles of a downward propagating beam will be refracted towards normal when passing through the ground surface. For ice, this can intensify the gain by about 3 dB. Conversely, normally incident rays reflected from subsurface interfaces that dip relative to a horizontal surface will refract toward horizontal when exiting the ground. For a layer refractive index = n, the layer dip, ϕ, must be less than $\sin^{-1}(1/n)$ to avoid this situation. For example, if $n = 1.7$ (dry sand or ice), then $\phi < 36^0$. For ice-saturated quartz sand, $\phi < 30^0$. If Martian mineralogy is iron-rich, then ϕ could be quite small. Although layers with ϕ near 30^0 may be unlikely, even small values of ϕ must be considered for space-borne radar platforms.

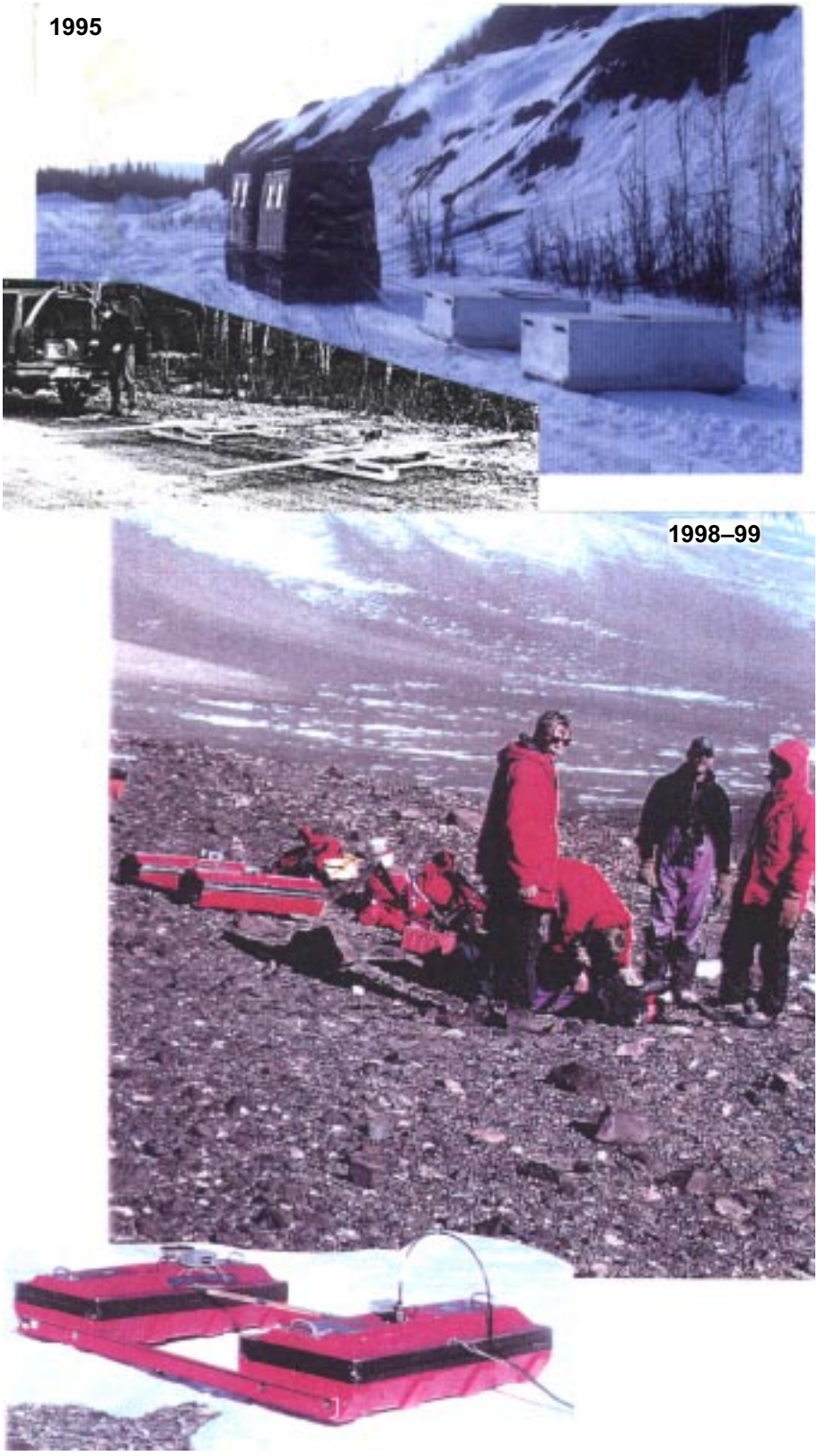

Fig. 1. Top: Shielded 50-MHz antennas under tow in the Fairbanks area of Alaska. Top inset: The 50-MHz antennas used for the Dry Valleys and which were unshielded. Bottom: Equipment and crew in the Dry Valleys. Largest surface rocks were usually 20–50 cm boulders of sandstone, granite and dolerite. Bottom inset: 100-MHz antennas.

Fig. 2. Location of Sloth Lake and Hjorth Hill in eastern Taylor Valley. White areas are glaciated, grey areas are valley bottoms, and dark areas are valley walls.

Fig. 3. Aerial photograph of the Sloth Lake area that contains the mound we profiled (arrow).

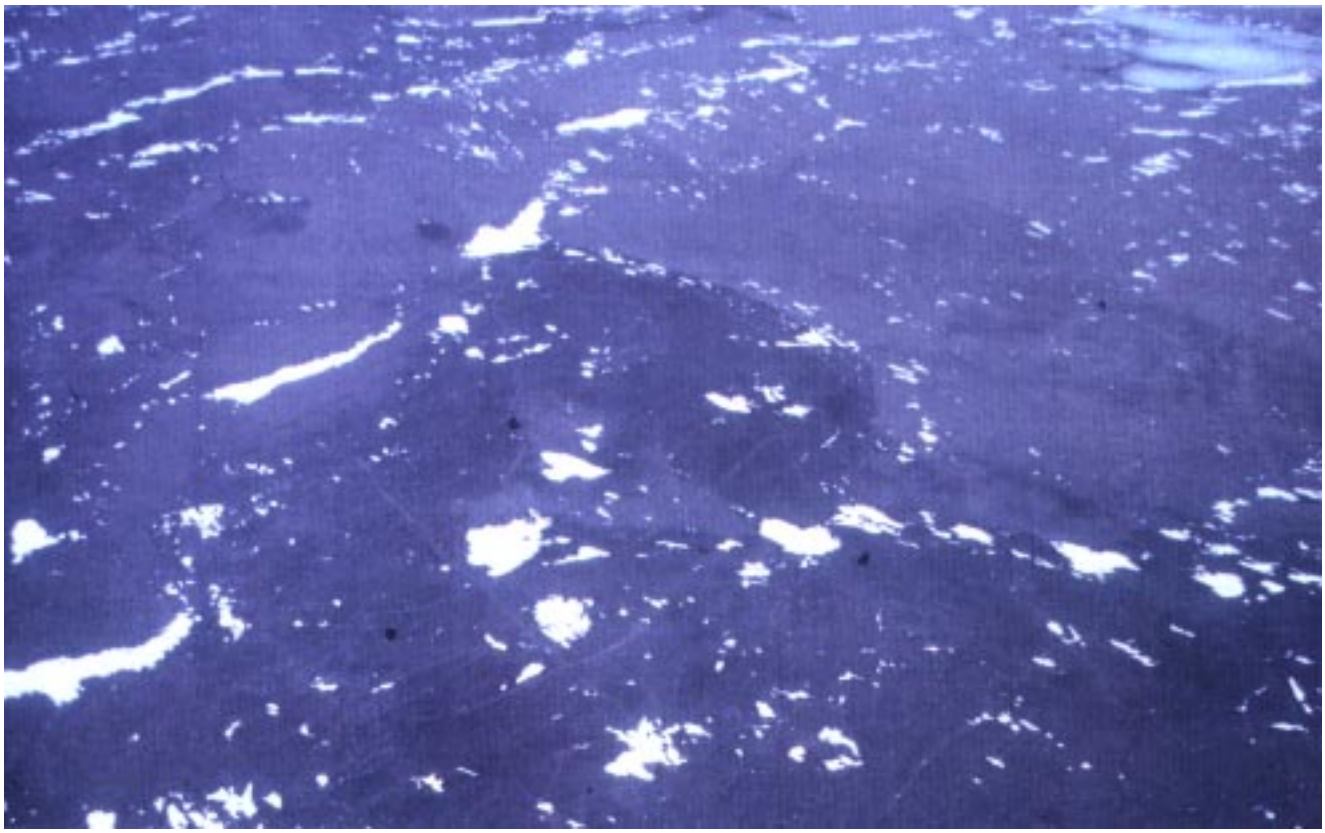

Fig. 4. Aerial photograph of the mound area showing our profile transects (faint lineations). The one discussed in Figure 5 ran from lower left to upper right.

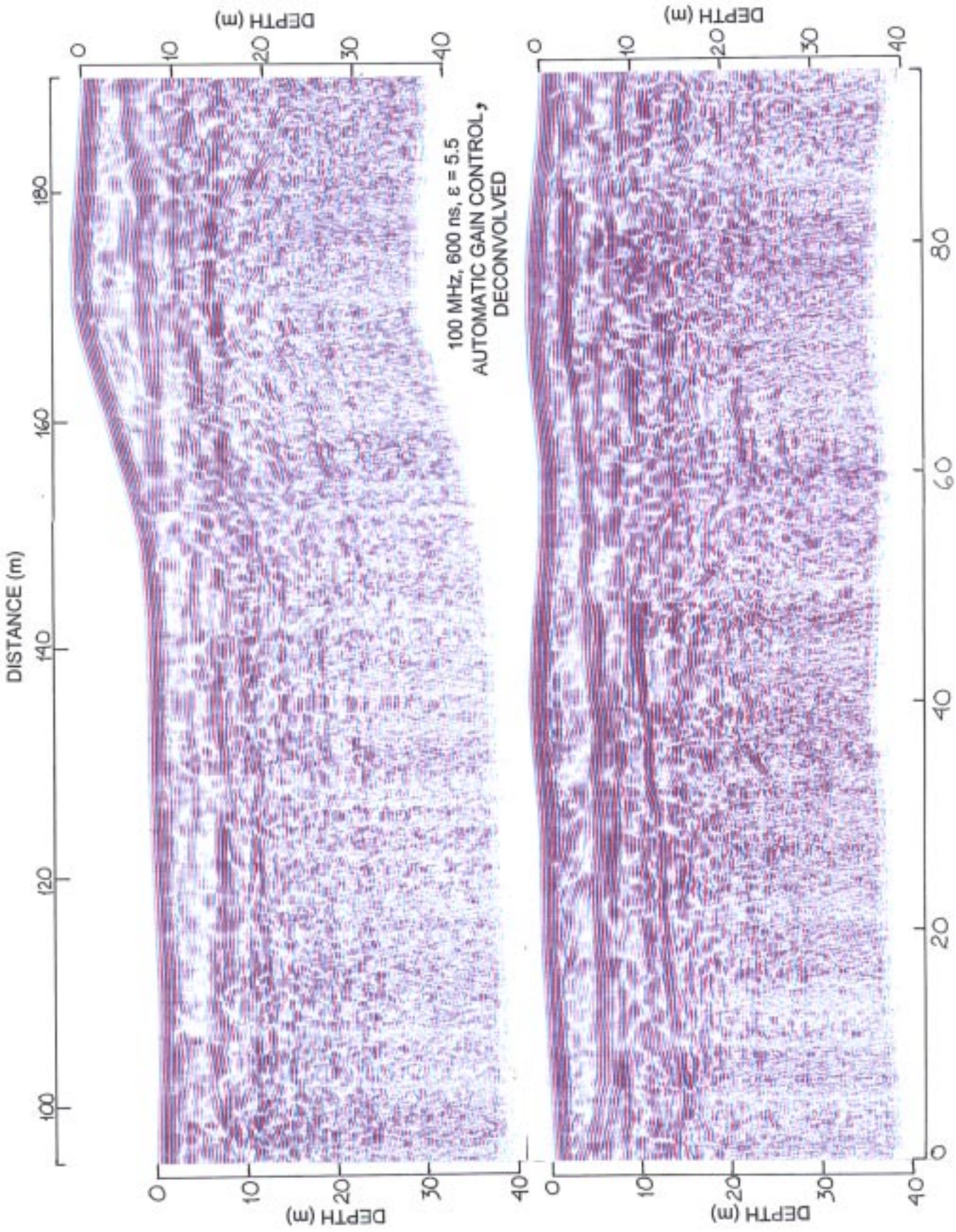

Fig. 5. 100-MHz profile of stratigraphy at Sloth Lake.

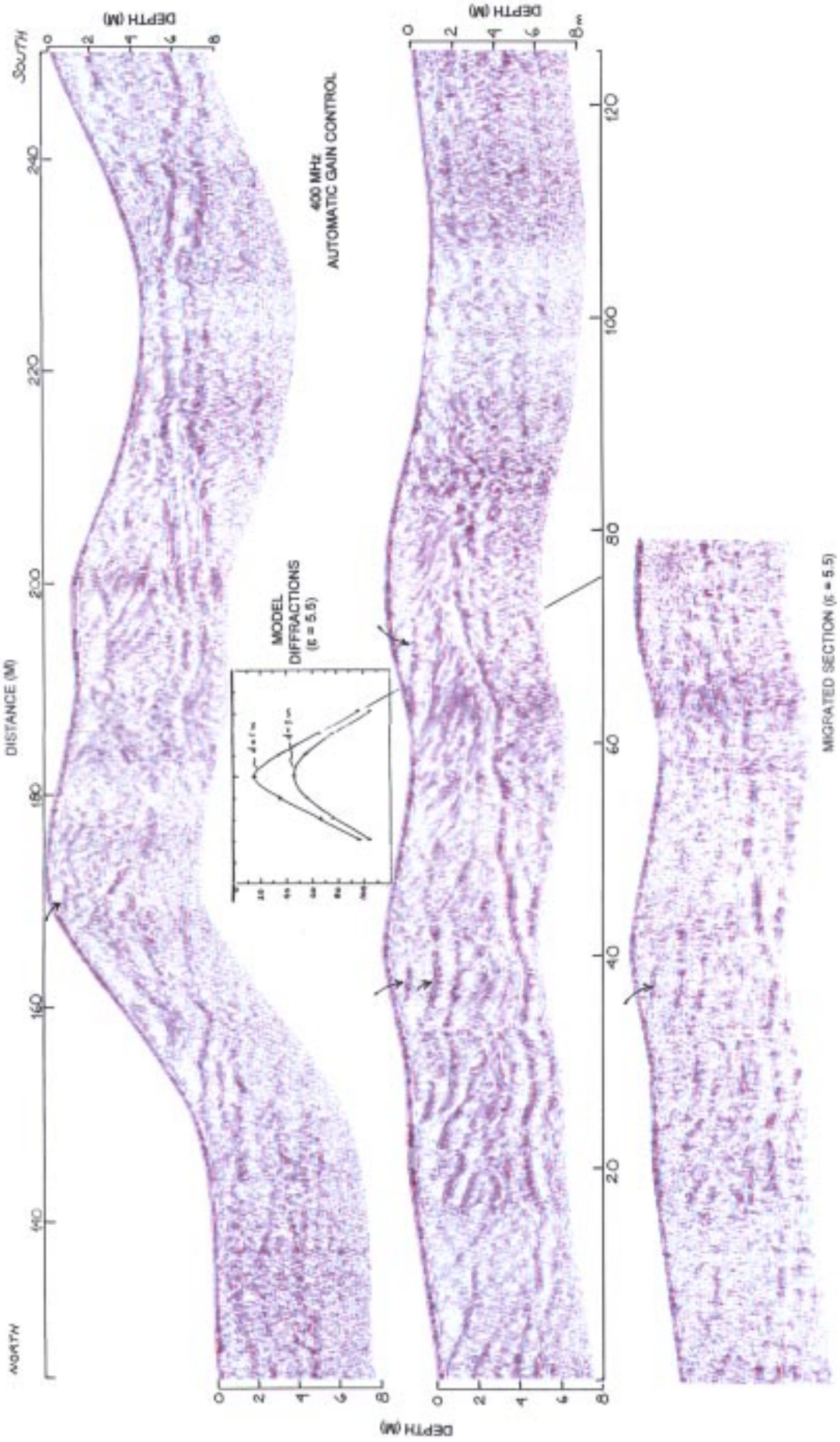

Fig. 6. 400-MHz profile of stratigraphy at Sloth Lake. The events in the profile are true reflection horizons because the model diffraction has a much steeper slope than any of them. Bottom profile is a 2-D migration of the section immediately above it. Small arrows indicate reflections from possible remnant ice from freeze front migrations.

Fig. 7. Aerial photograph of the Hjorth Hill area that includes the bifurcated mound structure (arrows) we profiled.

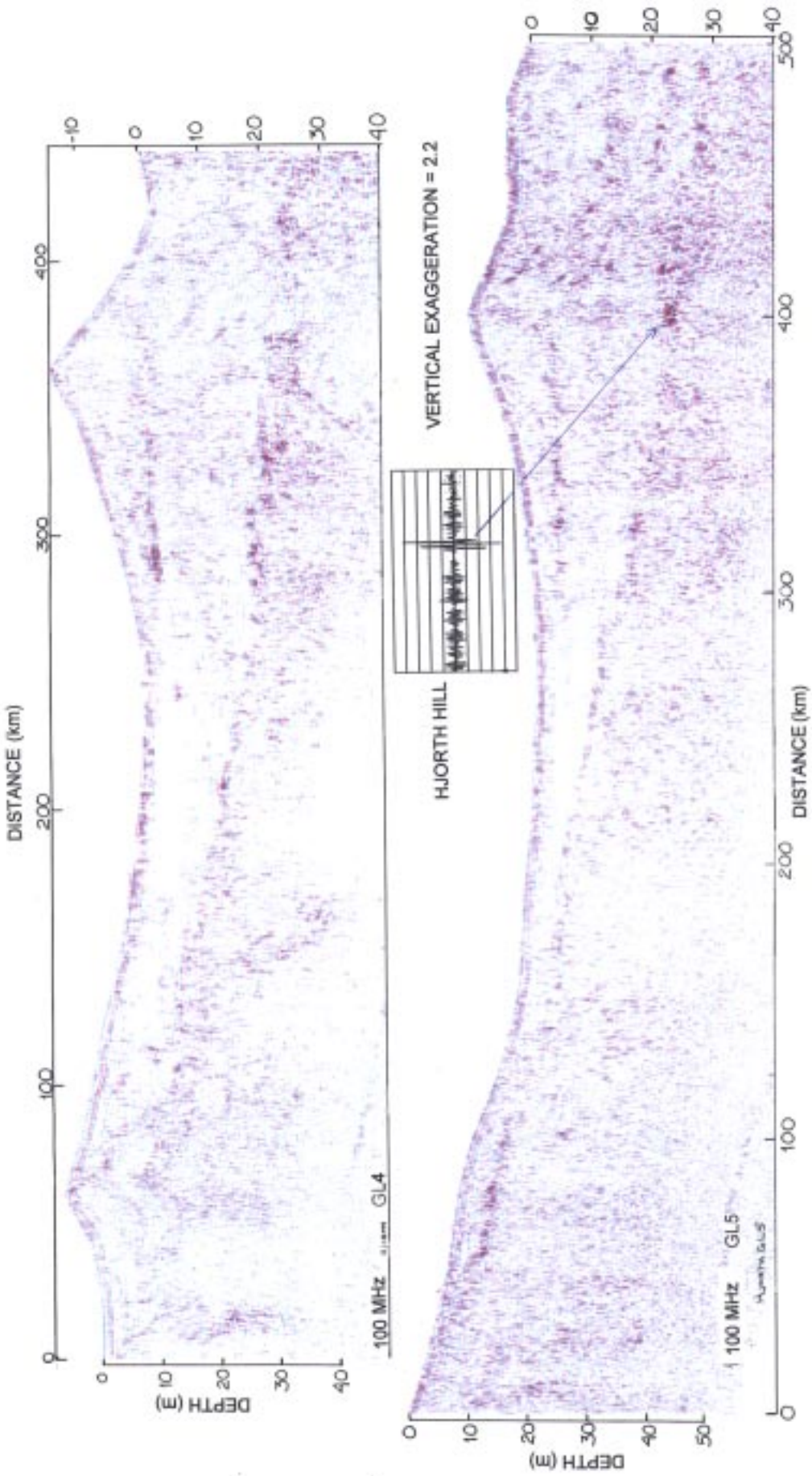

Fig. 8. 100-MHz profiles at Hjorth Hill. The inset trace shows a high signal-to-noise ratio for the deep event.

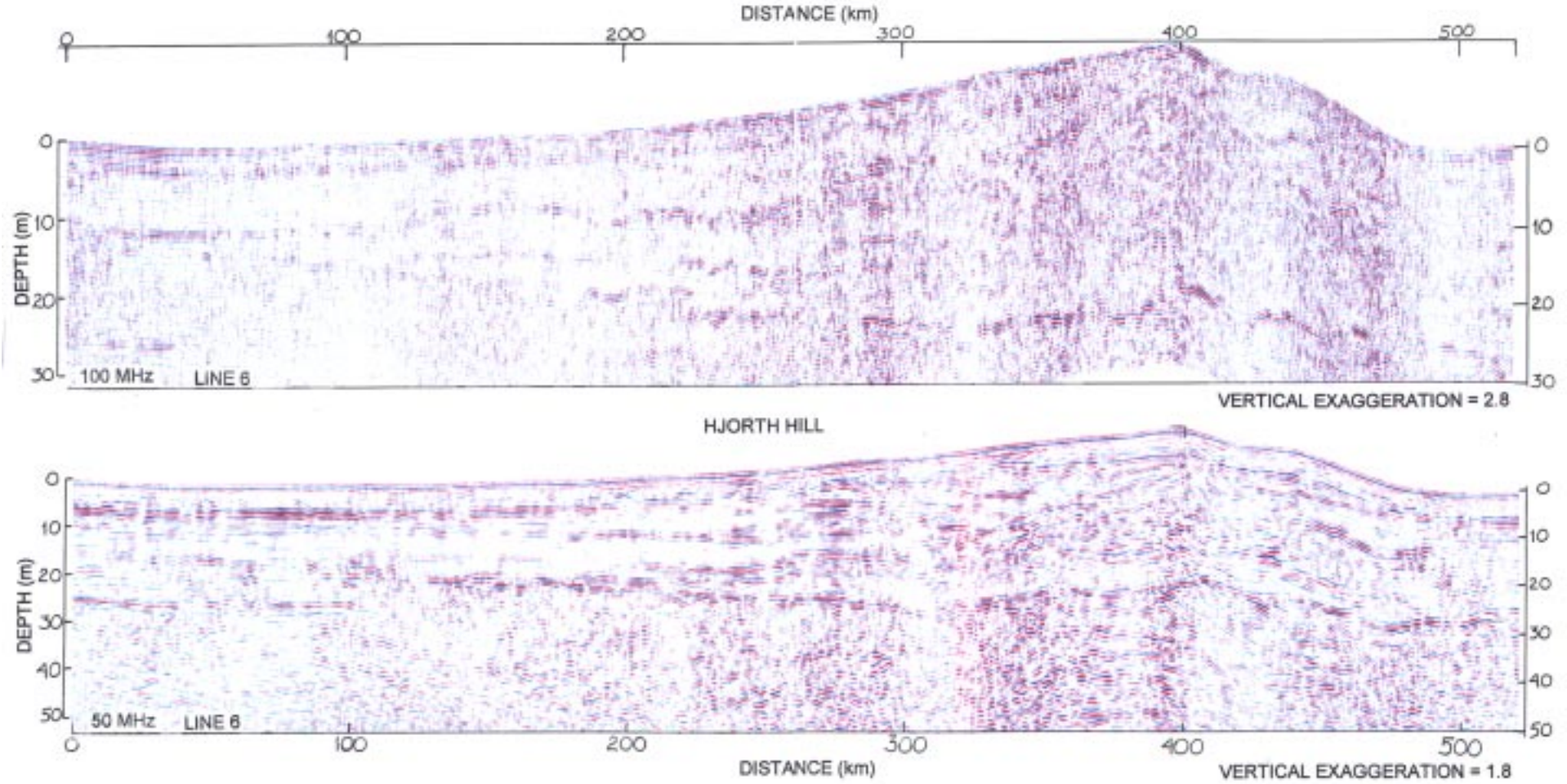

Fig. 9. Comparison between 50- and 100-MHz profiles across the same transect at Hjorth Hill. Both profiles show about 30–35 m penetration.

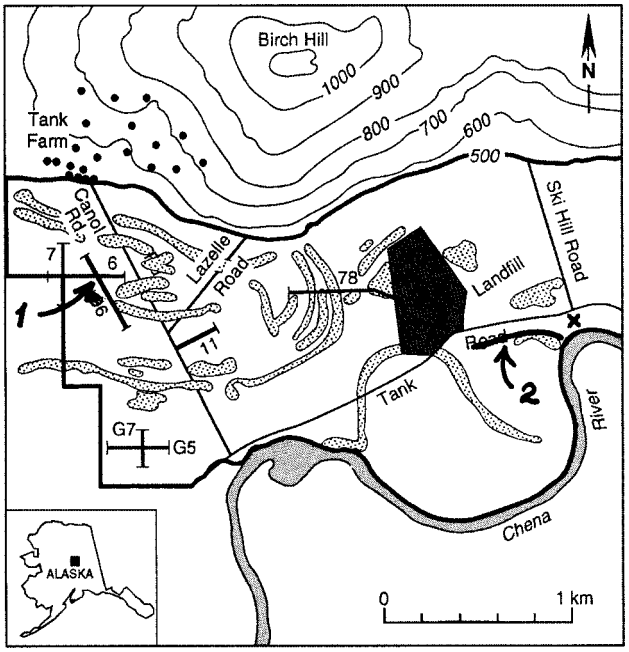

Fig. 10. Location of profiles (sites 1 and 2) on Fort Wainwright, in the Fairbanks area.

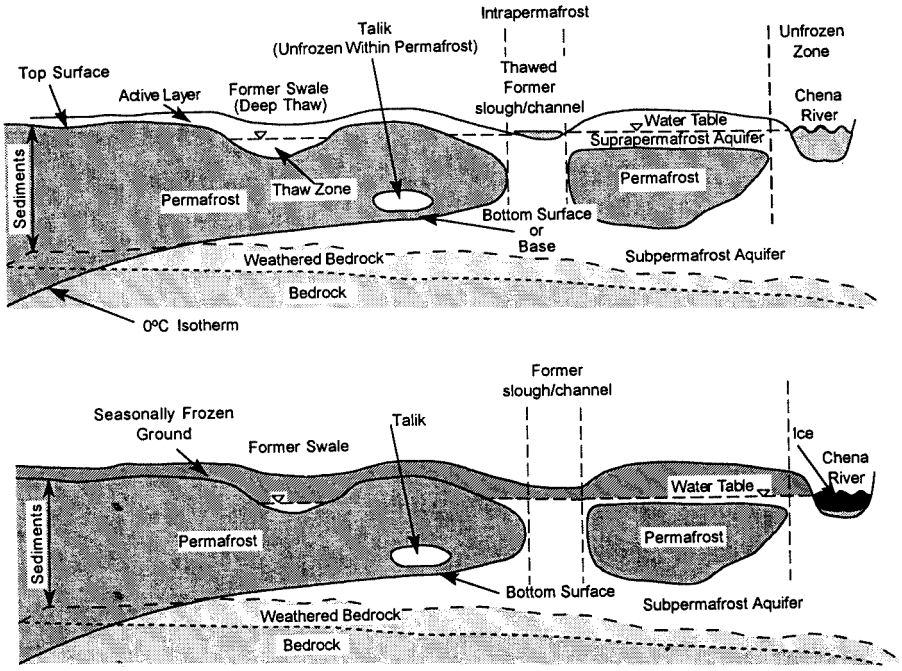

Fig. 11. Idealized sketch of the configuration and nomenclature for discontinuous permafrost and groundwater aquifers associated with it; (top) summer conditions, and (bottom) winter conditions.

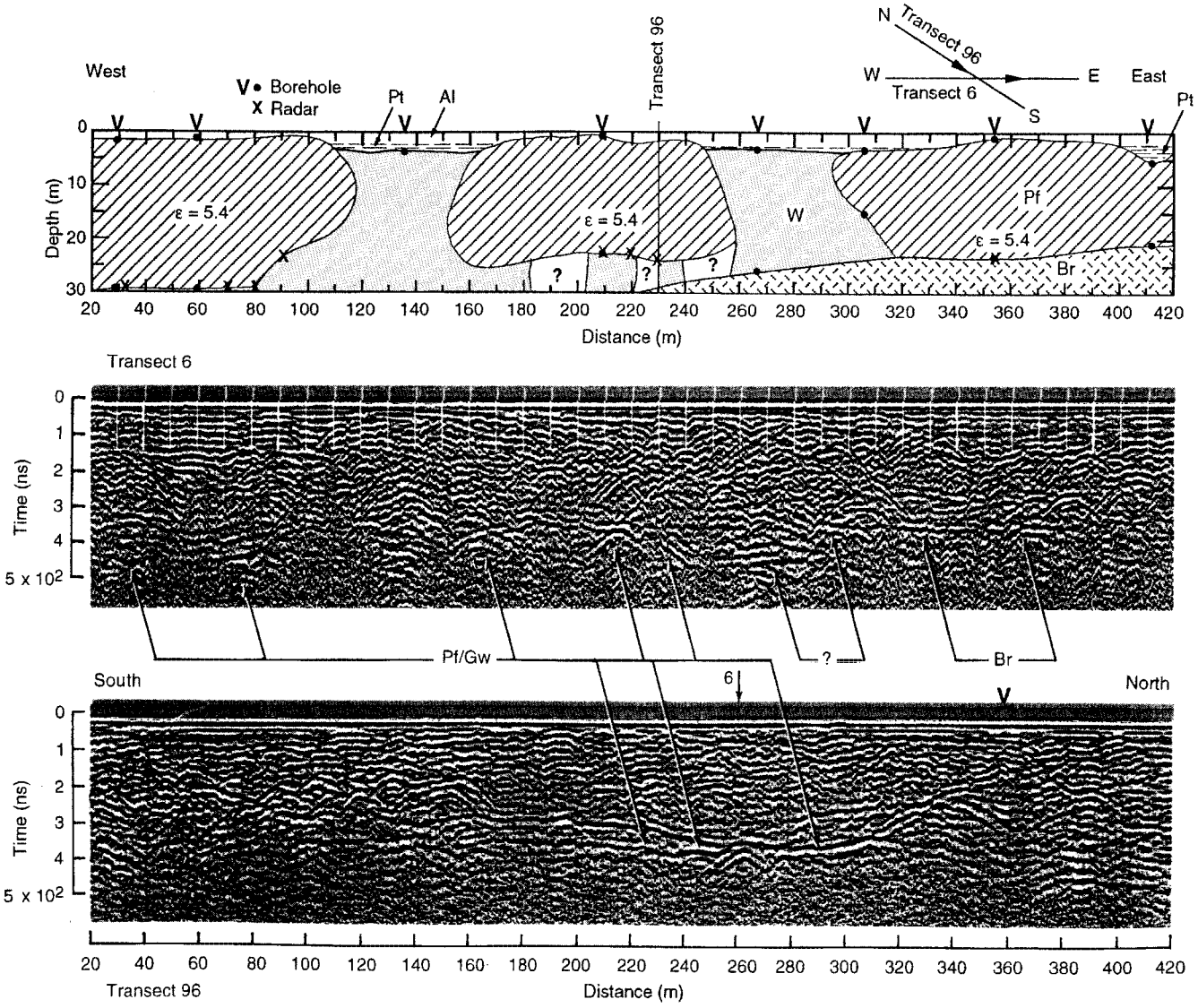

Fig. 12. 50-MHz profiles of two transects over discontinuous permafrost (site 1, Fig. 10), and an interpretation of transect 6 (from Arcone et al, 1998b). Subpermafrost groundwater appears discontinuous along transect 6, but continuous within 96. The symbols used are: Al, active layer; Pt, perennial thaw; Pf, permafrost; Br, bedrock; and Gw, subpermafrost groundwater. The question marks within the interpretation indicate probable unfrozen and unsaturated sediments; within the radar profile they indicate unexplained horizons in one of the interpermafrost thaw zones (W).

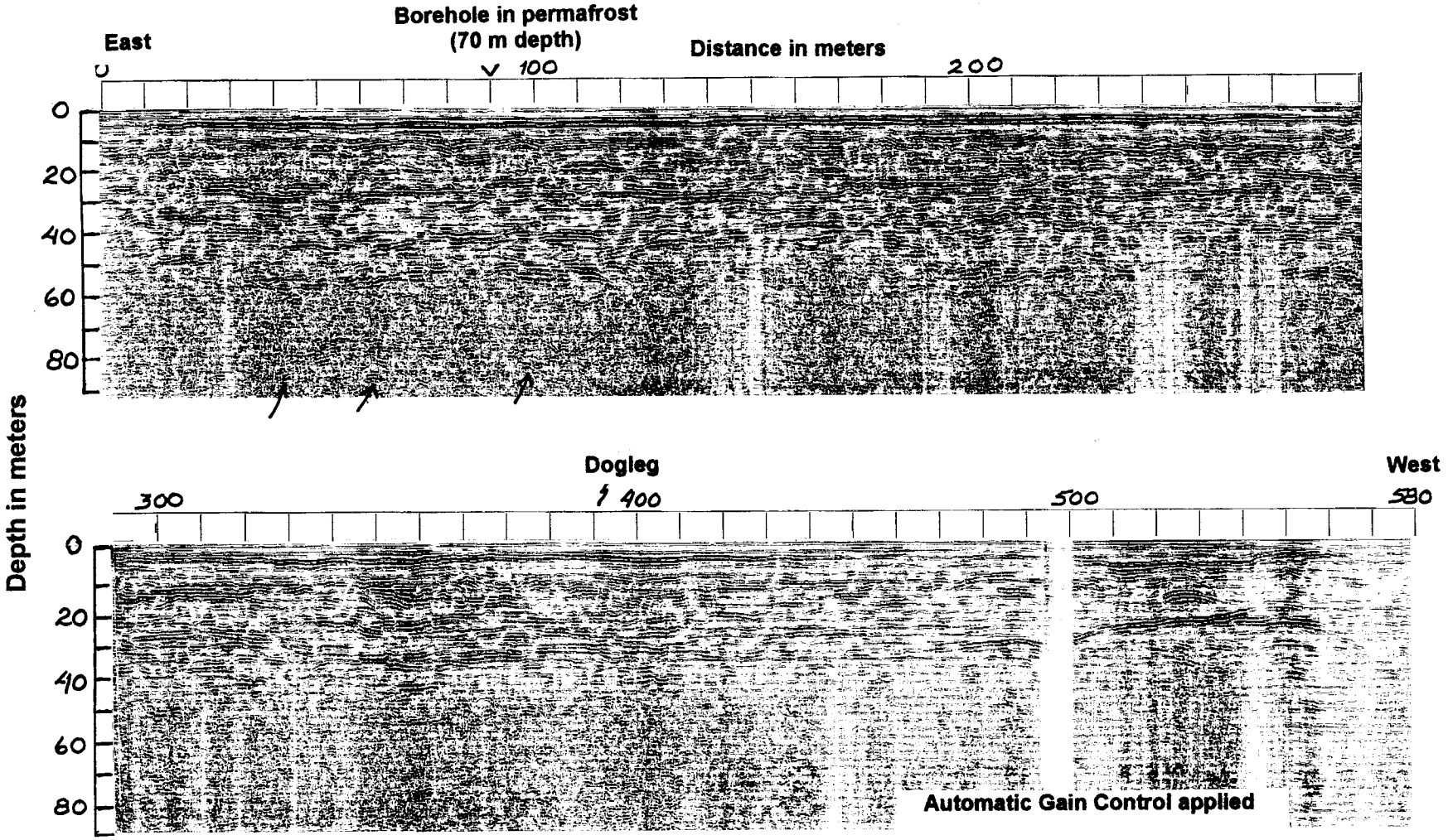

Fig. 13. 50-MHz profile from Fort Wainwright, near the Chena River. The arrows indicate deep reflections which may originate beneath the permafrost.

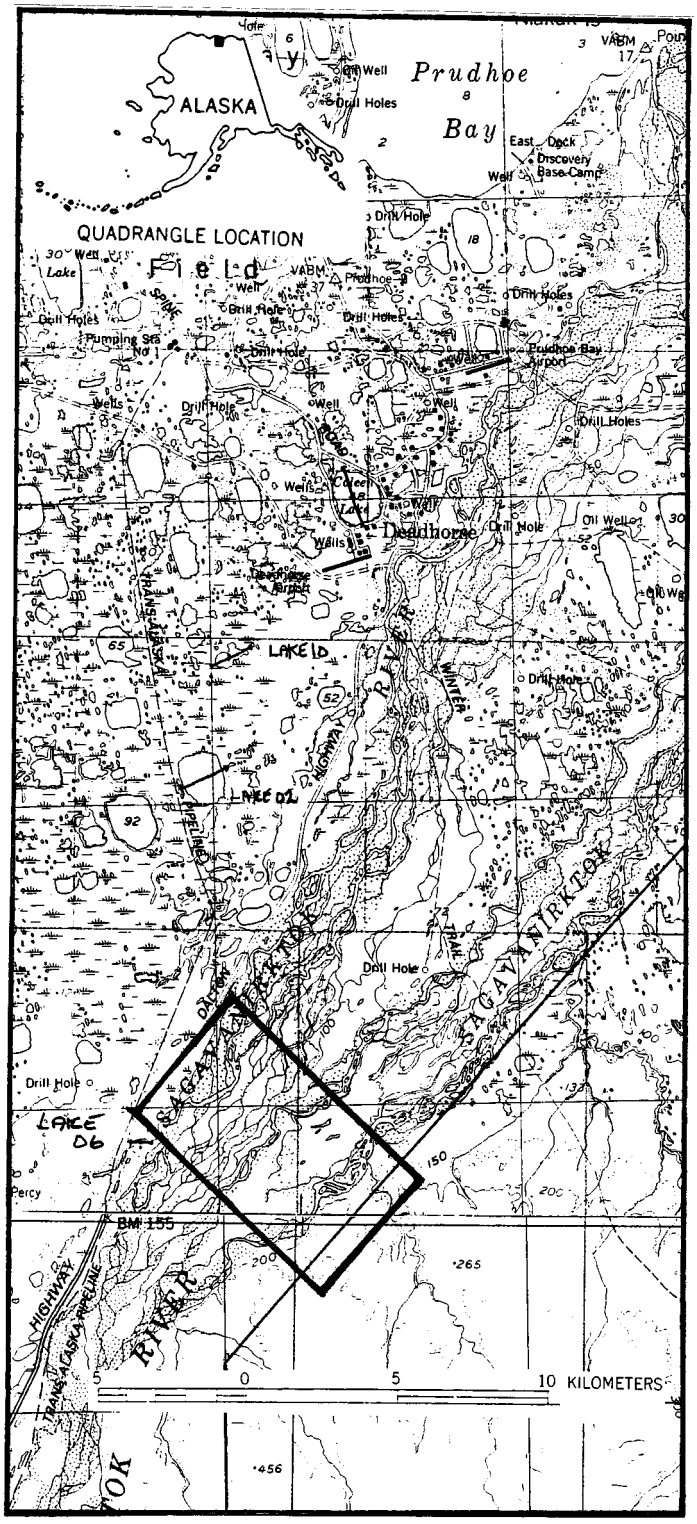

Fig. 14. Survey area on the Sagavanirktok River floodplain, about 25 km south of Prudhoe Bay.

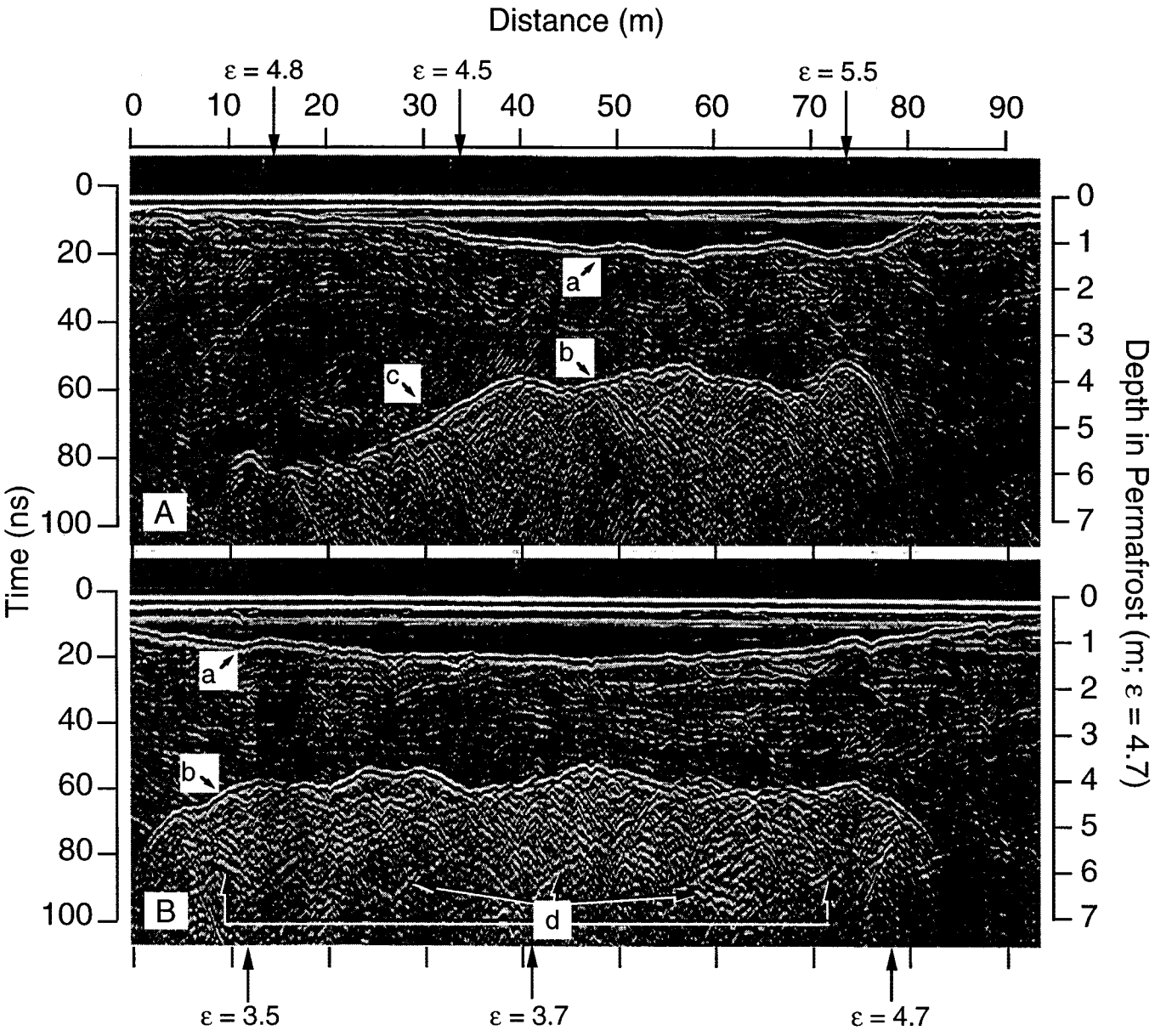

Fig. 15. Profiles along two sections of a control line. Vertical arrows locate boreholes where we calculated ε for the frozen alluvium above the talik. Labeled events are bottom of channel ice (a), talik surface (b), ice layer (c), bottom of talik (d). The direct coupling between antennas at 0 ns is the surface reference. The maximum ice thickness is 1.5 m in the top profile and 1.7 m in the bottom.

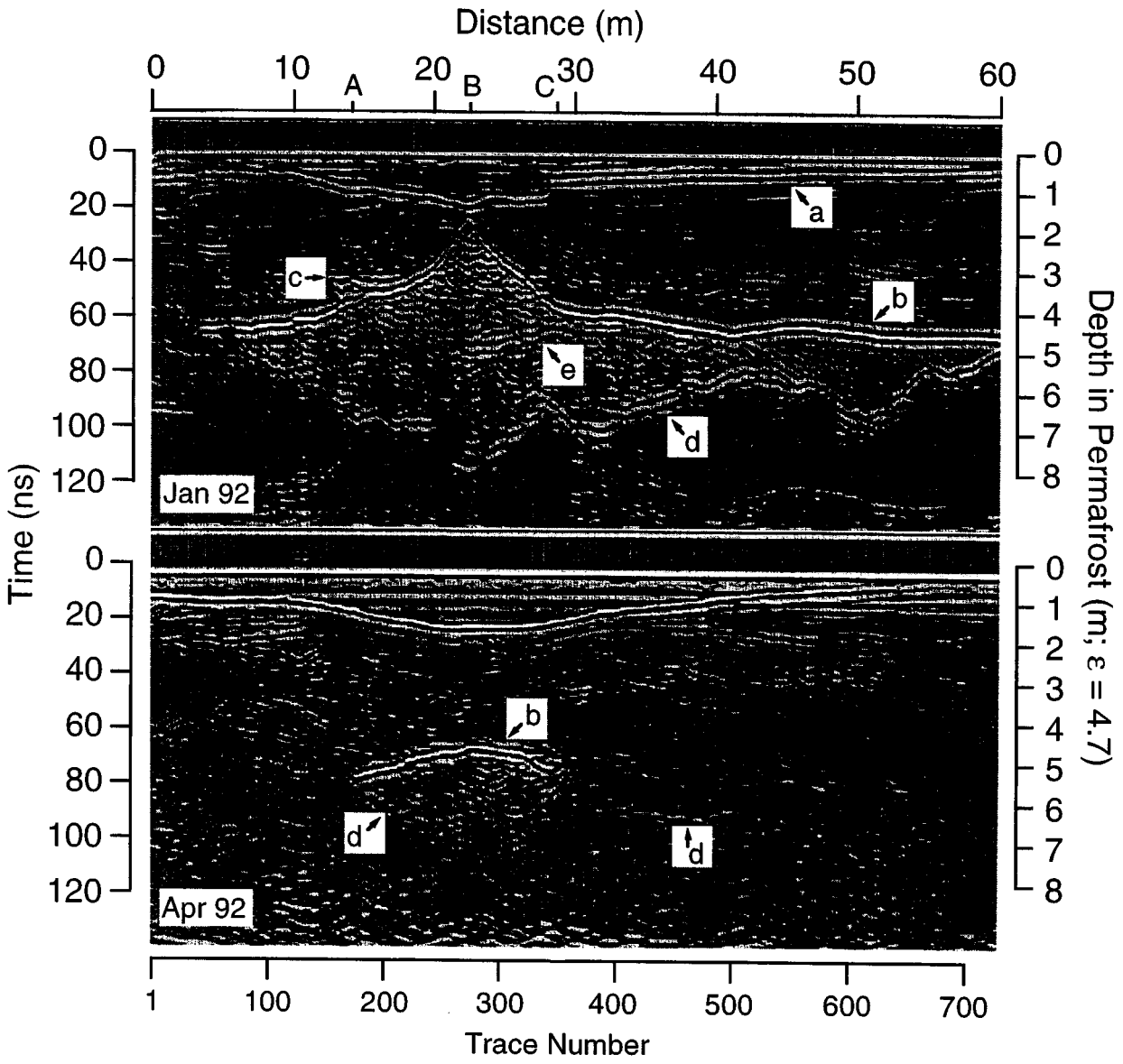

Fig. 16. Time-migrated seasonal profiles of a talik. Profile events are labeled as in Figure 15. I interpret the area within the talik above event (e) to be partially frozen. The maximum channel ice thickness (layer along top) is about 1.6 m.

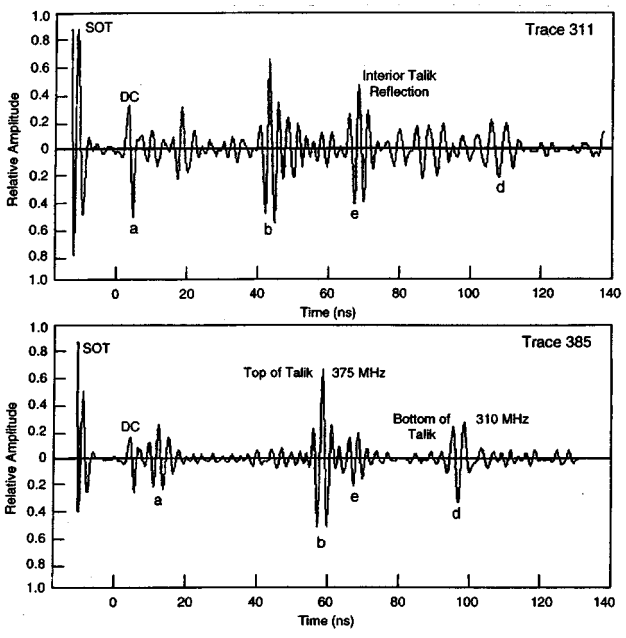

Fig. 17. Sample traces, with the same letter labels, from the January profile of Figure 16. Added gain makes the waveforms more visible. SOT (start-of-trace) is an artificial signal that triggers recording. DC, the direct coupling (partially filtered) between antennas, represents the channel ice surface. The reflections from the top and bottom of the talik have different phases. Trace 311, at 25 m distance, shows the strong reflection from within the talik. The phase agreement for the ice bottom, talik surface and internal talik reflections indicates increasing values of ε across each interface. The shift in local wavelet frequency to about 310 MHz (trace 385, at 30 m distance), is characteristic of propagation in a wet medium.

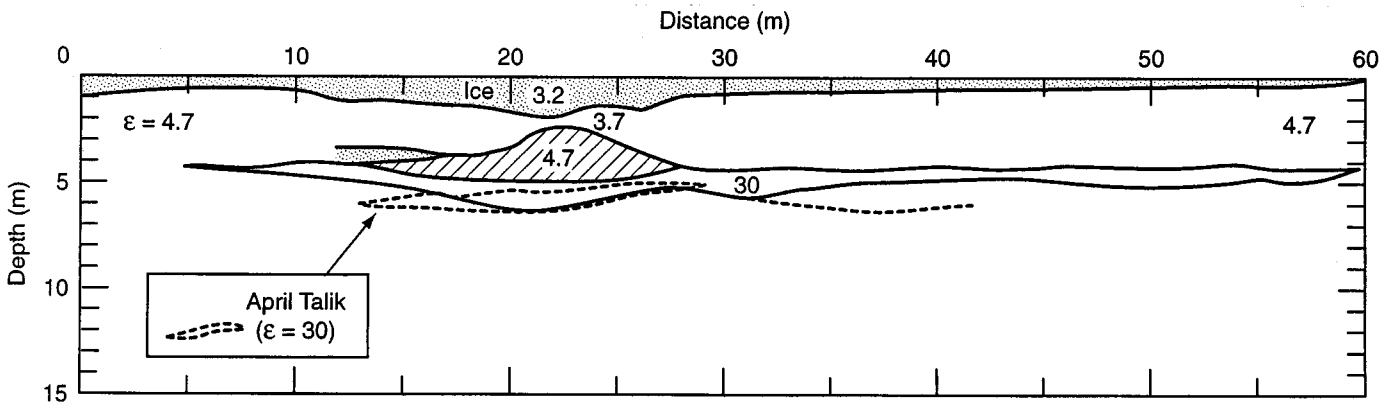

Fig. 18. Interpretations of the profiles in Figure 16. Permittivity values for each section are labeled. The cross hatched area is a partially frozen section of the January talik. The talik appears to have migrated deeper by April.